Hindawi
International Journal of Rotating Machinery
Volume 2019, Article ID 4396546, 13 pages
https://doi.org/10.1155/2019/4396546

Research Article

Investigation of Unsteady Aerodynamic Excitation on Rotor Blade of Variable Geometry Turbine

Jian Liu, Wei-Yang Qiao, and Wen-Hua Duan

Turbomachinery Aerodynamics and Acoustics Lab (TAAL), School of Power and Energy, Northwestern Polytechnical University, Xi'an 710072, China

Correspondence should be addressed to Jian Liu; liujian_npu@foxmail.com

Received 20 November 2018; Accepted 7 May 2019; Published 21 May 2019

Academic Editor: Funazaki Ken-ichi

To investigate the aerodynamic excitations in variable geometry turbines, the full three-dimensional viscous unsteady numerical simulations were performed by solving N-S equations based on SAS SST method. The aerodynamic excitations at varied expansion ratios with six different vane stagger angles that cause the unsteady pressure fluctuation on the rotor blade surface are phenomenologically identified and quantitatively analyzed. The blade pressure fluctuation levels for turbines with different vane stagger angles in the time and frequency domain are analyzed. As the results suggest, the blade excitation mechanisms are directly dependent on the operating conditions of the stage in terms of vane exit Mach numbers for all test cases. At subsonic vane exit Mach numbers the blade pressure fluctuations are simply related to the potential filed and wake propagation; at transonic conditions, the vane trailing edge shock causes additional disturbance and is the dominating excitation source on the rotor blade, and the pressure fluctuation level is three times of the subsonic conditions. The pressure fluctuation energy at subsonic condition concentrates on the first vane passing period; pressure fluctuation energy at higher harmonics is more prominent at transonic conditions. The variation of the aerodynamic excitations on the rotor blade at different vane stagger angles is caused by the varied expansion with stator and rotor passage. The aerodynamic excitation behaviors on the rotor blade surface for the VGT are significantly different at varied vane stagger angle. Spanwise variation of the pressure fluctuation patterns on is also observed, and the mechanism of the excitations at different spans is not uniform.

1. Introduction

Working condition of the aero-engine changes significantly within the flight envelops due to the variations of the flight mission of modern military aircraft, such as subsonic cruise, transonic speeding, and maneuvering. Variable cycle engine (VCE) is an effective way to enable the engine to obtain the optimal thermodynamic cycle and to acquire the good adaptability to various flight regimes [1]. VCE is a special type of aero-engine of which thermodynamic cycle can be adjusted by changing some components' shape, size, or position and the cycle parameters. The pressure ratio, mass flow, bypass ratio, and thrust can be varied between those of a turbojet and a turbofan engines, making it to combine the advantages of both. This kind of engine can be more effective at part-load or off-design conditions where the efficiencies are unacceptably bad with poor matching of the components owing to the fixed flow passage areas.

Variable geometry turbine (VGT) with adjustable vane stagger angle is proved to be the most effective way to alter the turbine characteristics to suit for the requirement of VCE [2]. Variable vane throat area is regulated with variable vane stagger angle; the flow capacity and expansion rate in high and low pressure stages could be changed to adjust the operating point of the engine.

Moffitt [3] summarized the experimental results of a single-stage turbine at different vane stagger angles found that the turbine efficiency reduces from the design vane case at all pressure ratios for either closed or open case. The turbine efficiency deduction at closed vane case is larger than the open case. Razinsky [4] presented the experimental results for the variable geometry turbine with design, closed, and open vane stagger angle conditions. They concluded that variable geometry turbine showed improved off-design performance. However, the numerical research of Bringhenti [5] showed

that the VGT improved turbine performances at the cost of reducing the surge margin of compressor component.

A new model based on linearization small deviation was proposed by Qiu [6, 7] to predict the steady-state performance of both single-stage and multistage turbines in VGT. The methodology is validated by the experimental data by Moffitt [3], and it is used to predict the performance characteristics of multistage turbines with variable geometry turbine.

Gao [8] proposed stepped spherical endwall concept in a high endwall angle power turbine to maintain constant endwall clearance at all turning angles. It was found that proposed endwall contouring could be applied to the variable geometry design of the power turbine, and the efficiency of the new-designed variable geometry power turbine kept nearly unchanged compared to the fixed geometry turbine. Due to the clearance between the blade and the endwalls for the rotation of the vane, the extra aerodynamic loss was introduced. Gao investigated the influence of the endwall clearance on the vane passage loss at varied vane stagger angles [9] and the effect of several flow control techniques to control the endwall loss [10–12].

Previous works lacked the detailed understanding of the mechanisms of the impact on the unsteady characteristics. Due to the relative motion of the neighboring blade rows, unsteady flow is inherent characteristic in turbomachinery. In turbine stages the upstream wake segments, upstream and downstream potential filed, and trailing edge shock impingement and reflection are the deterministic flow distortions which is seen by the blade [13, 14]. The periodic disturbance can significantly affect turbine performance and heat transfer, and it may lead to blade failure finally [13, 15]. And the unsteady aerodynamic excitations on the blade have received growing attention. The unsteady effect is recognized as a critical design parameter in the unsteady turbomachine design process.

As for the complex structure of the VGT due to the endwall clearance and the pivot enabling the rotation of the vane configurations, the structural strength of the vane is more important. The aerodynamic stimuli, i.e., the prediction, understanding the aerodynamic forces, are concerned in this study. The aerodynamic excitation mechanisms that drive the structural response in VGT are investigated.

2. Model and Numerical Setup

2.1. Calculation Model and Boundary Conditions. The unsteady computations are performed on a single-stage high pressure turbine of a low bypass ratio aero-engine. The detailed parameters of the high pressure turbine are listed in Table 1.

In the research of aerodynamic excitations in variable geometry turbine, the throat area of the turbine is adjusted through the change of the vane stagger angle to control the flow capacity of the turbine stage for different flight demands. The variable vane profiles are rotated around the vane trailing edge, as shown in Figure 1. The vane is named closed when the throat area of the vane is reduced with larger vane turning angle and vice versa, the corresponding throat area

Table 1: Design characteristics of the vane and rotor blade.

Parameter	Vane	Rotor
Z	27	84
Aspect ratio	0.56	1.57
$\gamma/^{\circ}$	55	46.4
R_{hub}/R_{tip}	0.855	0.833
P_{t0}/ KPa	2027.8	
T_{t0}/ K	1587.4	
$\Delta r/\%$		1
n/ r.min^{-1}		15217

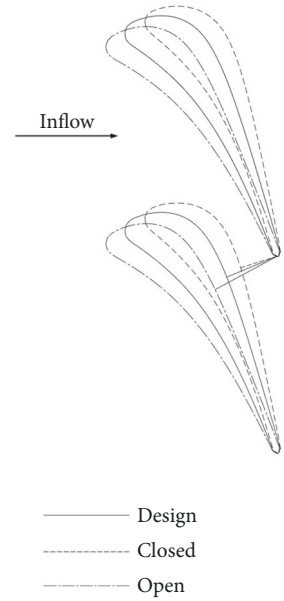

Figure 1: Variable vane positions.

is identified in Figure 1. In this study, six vane stagger angles corresponding to six vane throat area positions are investigated, i.e., design vane condition (0°), closed vane conditions (-2°; -5°), and open vane conditions (+2°, +5°, and +10°). It is noteworthy that the gaps between the vane and the endwall are not modelled in this study, and the effect of the clearance at the blade endwall will be included in the future work.

Unsteady simulations of VGT are performed under four total-to-static pressure ratios for each vane stagger angle position; the total-to-static pressure ratios are, namely, low (1.56), medium (2.25), nominal (3.41), and high (4.50) expansion ratio conditions. The operating conditions of VGT including degree of reaction (Ω), stage loading factor ($\Delta H/U^2$), and flow coefficient (C_a/U) with nominal pressure ratio are listed in Table 2.

Domain scaling method is adopted to satisfy the requirements of the periodic boundary conditions. The vane number is adjusted from 27 to 28 with scaled vane profile. Accordingly, the domain in the research could be simplified to 1/28 annulus consisting of one vane and three rotor passages. The schematic of the computing domain is shown in Figure 2.

Table 2: Operating conditions for VGT with nominal pressure ratio.

Vane turning angle	P_{t0}/P_{s2}	Re_c	Ma_1	$Ma_{2,r}$	Ω	$\Delta H/U^2$	C_a/U
-5°	3.41	5.38×10^5	1.36	0.62	0.04	2.26	0.48
-2°	3.41	6.81×10^5	1.32	0.74	0.11	2.27	0.55
0°	3.41	7.76×10^5	1.26	0.82	0.16	2.28	0.57
+2°	3.41	8.69×10^5	1.19	0.92	0.27	2.40	0.57
+5°	3.41	1.01×10^6	1.01	1.02	0.42	2.24	0.54
+10°	3.41	1.19×10^6	0.79	1.38	0.69	1.97	0.53

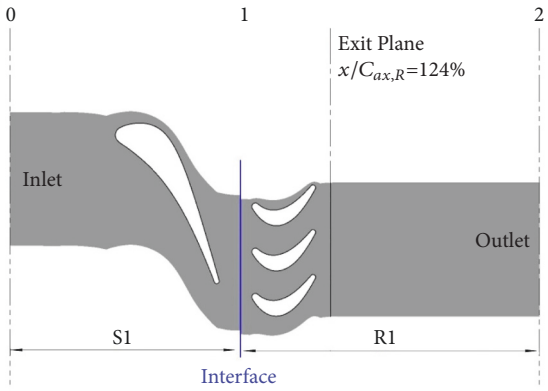

Figure 2: The computational domain in this study.

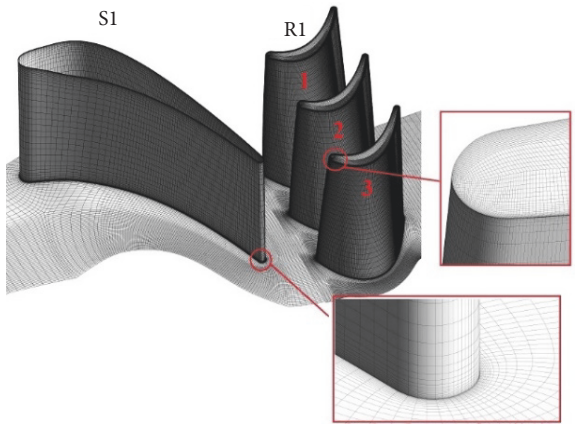

Figure 3: Computation grid in this study.

The inlet of the domain is placed at one $C_{ax,S}$ upstream of the vane LE plane, the outlet section I extended to 3.5 $C_{ax,R}$ downstream the rotor TE, which are subscripted as sections 0 and 2, respectively.

Pressure-inlet boundary condition with total pressure distribution along spanwise is given accompanied with total pressure, and the free stream turbulent intensity is set as 10%. Average static pressure considering radial equilibrium is applied at the outlet boundary, of which the values are listed above. Adiabatic nonslipping wall conditions are adopted on the blade surfaces and endwalls. Rotational periodicity is employed in the circumferential direction.

2.2. Numerical Method and Computation Grid. Three-dimensional unsteady calculations are performed by ANSYS CFX 17.0 software. Shear Stress Transport (SST) k-ω model is selected as the turbulence model in the steady-state simulation due to its superiority in the precise simulation in rotating turbomachinery [16]. Subsequently, the forgoing steady-state solutions serve as initial values for the unsteady simulations. Due to the complexity of the flow structure and the unsteady interaction, the RANS/LES hybrid model method Scale-Adaptive Simulation (SAS) [17, 18] is adopted in the unsteady simulation. The detailed description of the numerical method is discussed in our previous work [19].

CFX Turbo-Grid is used to generate the structured computation grid; the blade flow path is H-O-H grid. The 3D view of the mesh is illustrated in Figure 3.

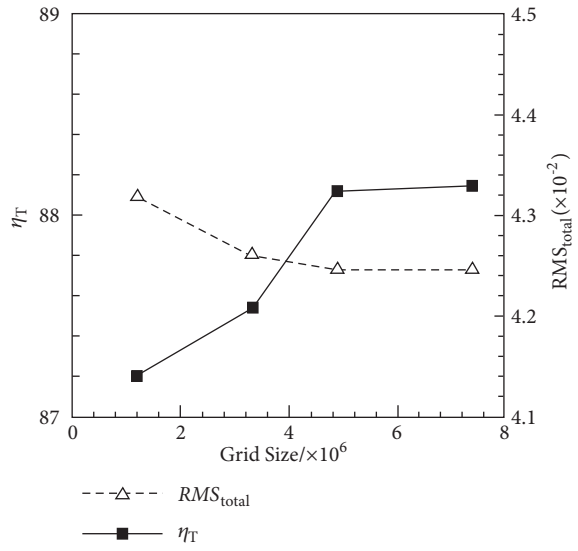

Figure 4: Grid sensitivity analysis for straight vane case.

The grid independency check is conducted by unsteady simulation on the design (0°) vane case at high pressure ratio condition with varying grid sizes ranging from 1.2 to 7.4 million nodes. The results of the grid independency check are shown in Figure 4.

Total-to-total turbine efficiency (η_T) and global pressure fluctuation intensity (RMS_{total}) both change significantly with increasing grid numbers in Figure 4. Integration of

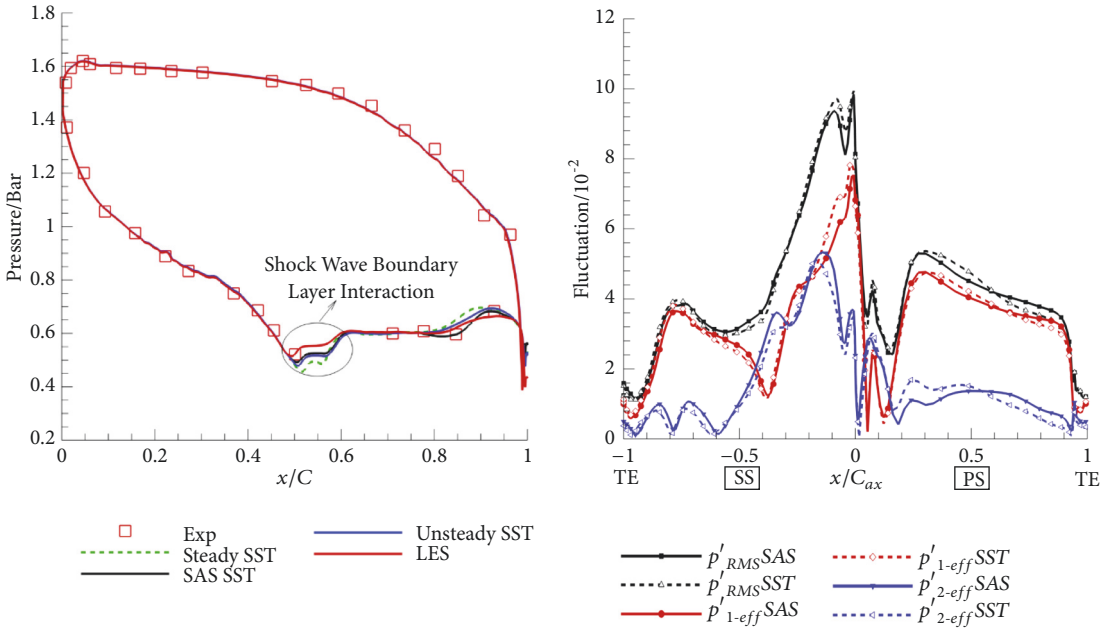

(a) Steady pressure distribution

(b) Unsteady pressure fluctuation distribution

Figure 5: Validation of numerical models.

the RMS value of the fluctuating pressure along the blade is calculated to measure the global pressure fluctuation strength; RMS_{total} is defined as

$$RMS_{\text{total}} = \sqrt{\frac{\int_{\text{arc}} \left(\sum_{i=1}^{m} p_i'^2\right) \mathrm{d}s}{m \int_{\text{arc}} \mathrm{d}s}}, \quad (1)$$

It is suggested that the grid independence of the predicted turbine efficiency could be satisfied with 5 million grid nodes. The predicted RMS_{total} keeps almost constant when the grid size is beyond 3.3 million. The mesh with 5 million grid nodes is finally selected to study the aerodynamic excitations of the VGT.

2.3. CFD Verification. The experimental data from the transonic high pressure turbine in literature [20] are used to validate the accuracy of the CFD model in this study. Detailed checks have been conducted in our previous literature [19], and the results are presented in Figure 5(a). It is suggested that both unsteady SST and SAS SST models can capture the plateau pressure pattern in the shock wave boundary layer interaction (SWBLI) region, but the prediction of the SAS SST model is more accurate.

Considering that the paper focused on the unsteady excitations, a comparison of SAS SST and URANS SST for unsteady pressure fluctuations is given in Figure 5(b). Figure 5(b) suggests that the results of the two models agree well generally, especially for the overall pressure fluctuation and the pressure amplitude of 1BPF. So in this paper, the SAS SST model is adopted to predict the unsteady pressure excitations on the rotor blade of VGT.

3. Identification of Pressure Fluctuations on Rotor Blade

The adverse work environment of the transonic turbine blade, especially for the rotor blade, may cause high cycle fatigue (HCF) and breakdown of the machine. The periodic disturbances originate mainly from the potential field interaction of the adjacent blade rows, the upstream wake traveling, and the TE shock wave from the upstream vane.

In this section, the unsteady aerodynamic excitations at midspan of the rotor blade with design vane stagger angle (0°) are analyzed. Three issues are addressed: Firstly, the interpretation of the blade pressure fluctuations with respect to the surrounding unsteady distortions, ideally linking the observed blade surface pressure fluctuations to their corresponding excitation sources. This is achieved by comparing instantaneous pressure fluctuation contours of the blade passages with space-time plots of pressure fluctuation enabling to track the movement of the excitation source through the passage. Secondly, quantification of blade excitation mechanisms in both the frequency and time domains for the design vane stagger angle case by Fourier transformation of the surface pressure. Thirdly, the discussion and analysis of the overall aerodynamic excitation levels with respect to various total-to-static pressure ratios.

Figure 6 presents the pressure fluctuation scaled with total pressure the stage inlet at midspan of rotor blade no. 2 in two successive vane passing periods (Ts) at total-to-static pressure ratio of 1.56 and 3.41, the corresponding vane exit Mach numbers are 0.76 and 1.27, respectively. The abscissa of the space-time figure is the time coordinate normalized by the vane passing period. The ordinate represents the blade axial

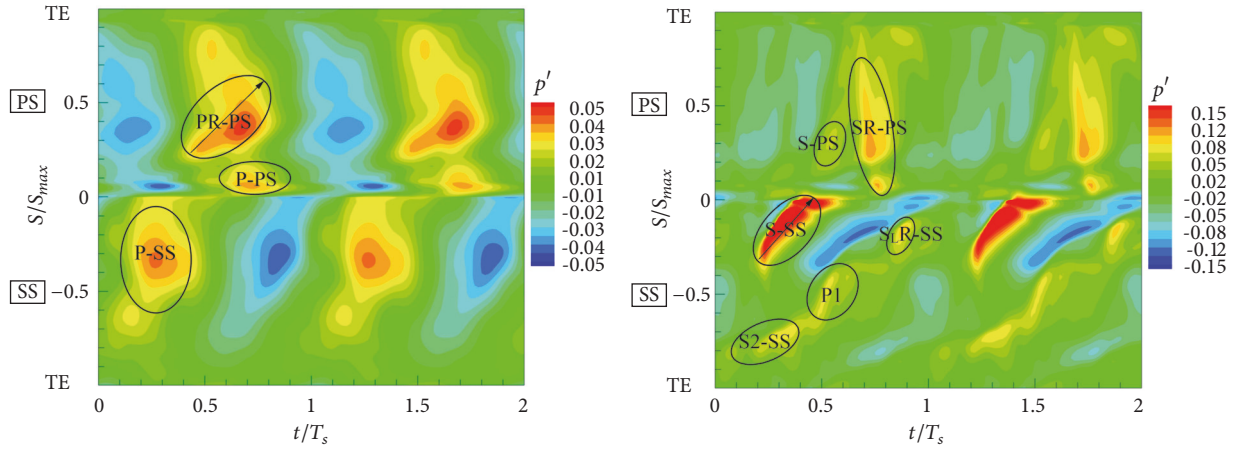

(a) P_{to}/P_{s2}=1.56, midspan (b) P_{to}/P_{s2}=3.41, midspan

FIGURE 6: Space-time plots of unsteady pressure at midspan of the rotor blade surface.

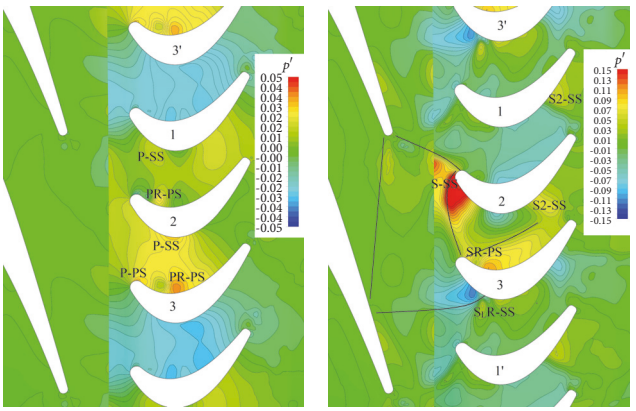

(a) t/Ts=0.4, P_{to}/P_{s2}=1.56 (b) t/Ts=0.4, P_{to}/P_{s2}=3.4

FIGURE 7: Instantaneous pressure fluctuation contour at rotor midspan at low and nominal pressure ratio operating conditions.

chord from the leading edge (0) along suction (negative half) and pressure (positive half) side to the trailing edge (1) at one instant in time. The shape of the pressure events in the space-time plot provides valuable information about characteristic motions associated with the fluctuations.

Above all, the relation of the space-time plot of the unsteady pressure around rotor blade and the instantaneous pressure fluctuation contour at rotor passage should be clarified. The phase difference of the pressure fluctuation on rotor blades nos. 3 and 1 in Figure 7 is ±0.333 Ts in the space-time plots of the pressure fluctuation around rotor blade no. 2 in Figure 6.

At low expansion ratio condition, no vane TE shock is present and the rotor blade unsteady pressure peaks are entirely related to the periodical experience of the upstream vane potential field and the wake propagation within the rotor passage.

Only one pressure fluctuation peak designated as P-SS is observed on the rotor blade suction side, which is relevant to the impact to the potential excitation from the upstream vane. Alternately experiencing of the high and low pressure regions of the upstream vane potential field serves as the potential excitation source on the rotor blade. The excitation mechanism is indicated in Figure 7(a), showing the instantaneous pressure fluctuation contour in the rotor passage at midspan. When the wake segments convectively propagate through the rotor passage, the unsteady pressure events will appear as inclined lines in the space-time plot, which is obviously not the dominant effect at low expansion ratio conditions on the rotor suction side. This indicates that the pressure excitation on the rotor suction side is mainly caused by the vane potential excitation.

Two pressure fluctuation peaks are seen on rotor pressure surface, namely, P-PS and PR-PS, which are strongly influenced by the upstream potential field. The pressure fluctuation peak P-PS at the front pressure side is related to the direct impact of the vane potential interaction, and the range and amplitude of the unsteady pressure event are lower than the pressure fluctuation peaks P-SS and PR-PS. The pressure fluctuation peak PR-PS is due to the reflection of the vane potential interaction from the suction surface of the neighboring blade. The time delay between the pressure

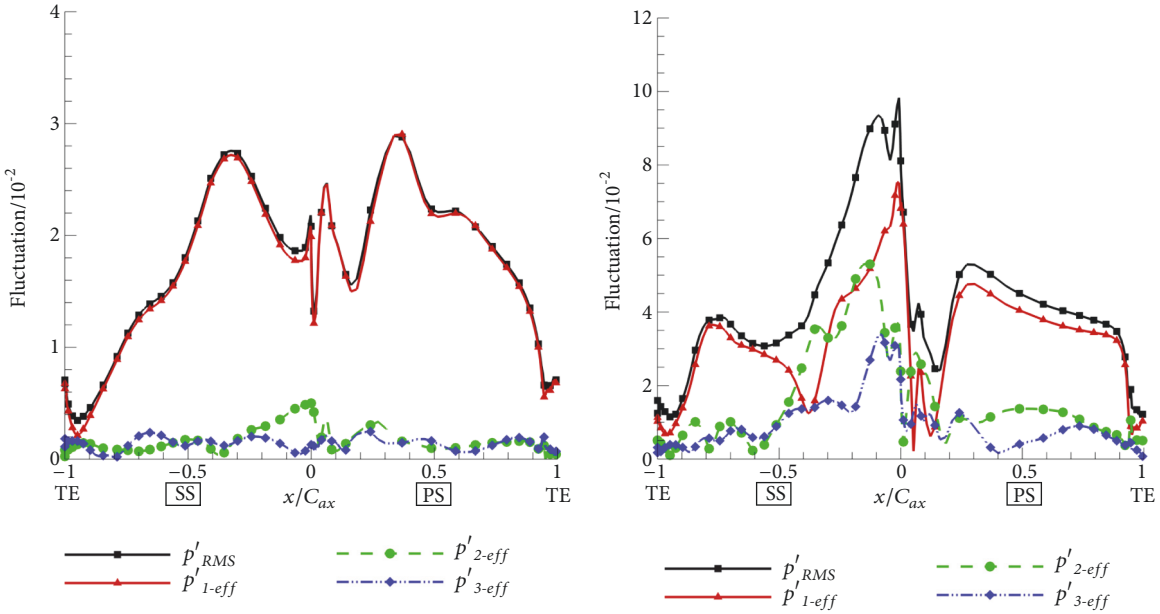

(a) P_{to}/P_{s2}=1.56 (b) P_{to}/P_{s2}=3.4

FIGURE 8: Unsteady pressure amplitude distribution along rotor blade surface at midspan.

fluctuation peak PR-PS and P-SS is due to the traveling of the wave front across the passage. The effect of wake segment traveling through the rotor blade passage is visualized on the rotor pressure side, causing the pressure fluctuation peak PR-PS to propagate along the rotor blade surface toward the TE as a pressure wave. The motion induced by wake propagation is marked with an arrow in Figure 6(a). Therefore, at the low expansion ratio operating condition in Figure 6(a), potential field excitation and wake excitation are the main sources of the rotor blade pressure excitations.

At nominal expansion ratio operating condition, the flow at the vane exit is transonic. The excitation levels on the rotor blade are several times of the low expansion ratio condition in Figure 6(b). The pressure fluctuation peaks are relevant to the motion of the vane TE shock in the rotor passage. The right running stator TE shock impinges on the rotor blade crown and moves to the rotor LE and a strong pressure fluctuation peak designated S-SS is formed. The shock motion is indicated with an arrow in Figure 6(b), and the corresponding pressure distortion events are shown in Figure 7(b) with the instantaneous unsteady pressure contour. Expansion with pressure drop follows the shock. The pressure peak named SR-PS on the pressure side origins from the shock reflection of the incident shock S-SS as it impinges on the rotor suction side of the neighboring blade. The reflected shock can be seen on the rotor blade no. 3 at t/Ts=0.4 in Figure 7(b), corresponding to t/Ts=0.733 in the space-time plot in Figure 6(b), and the shock system is marked with black lines. When the vane trailing edge shock passes through the rotor leading edge and reaches the front of the pressure side, the needed rotation of the fluid exceeds the maximum achievable rotation angle for an oblique attached shock. It bows around the leading edge and influences the pressure side for a short time period, named S-PS, of which the peak value is lower. At the front suction side, another narrow region of high pressure fluctuation level named S_LR-SS is noticed. It is caused by the reflection of the left running vane TE shock, and the excitation mechanism is indicated in Figure 7(b). The pressure fluctuation peak designated S2-SS is due to different strength of the rotor exit shock wave. The pressure fluctuation peak P1 at rotor suction surface is due to the variation of the shock wave strength in the rotor passage.

It can be concluded from Figure 6 that in principle all pressure peaks can be associated with the vane TE shock motion in the rotor passage. The vane TE shock excitation is dominant on the rotor blade at the high expansion ratio condition. Potential field and wake excitations are certainly existent but overlaid by the vane TE shock excitation.

To analyze the pressure fluctuation level on the rotor blade surface qualitatively, Figure 8 presents the pressure fluctuation amplitude levels along the midspan of the rotor blade surface at low and nominal expansion ratio conditions. In this figure, p'_{RMS} represents the RMS value of the pressure fluctuation normalized with the total pressure at stage inlet $p' = (p - \overline{p})/P_{01}$. The pressure field was Fourier transformed in time along the rotor blade, $p'_{n-eff} = p'_{n-\mathrm{amp}}/\sqrt{2}$ represents the effective value of the pressure fluctuation related to the nth blade passing frequency (BPF) in frequency domain, and $p'_{n-\mathrm{amp}}$ is the pressure amplitude of the nth BPF.

Compared with the low expansion ratio operating condition, the appearance of the vane TE shock gives a rapid rise of the pressure fluctuation amplitude level along the rotor blade surface. At low expansion ratio condition, three pressure fluctuation peaks at low expansion ratio condition caused by the potential field and wake excitations, namely, P-PS, PR-PS, and P-SS, are of the same order of the magnitude. In the

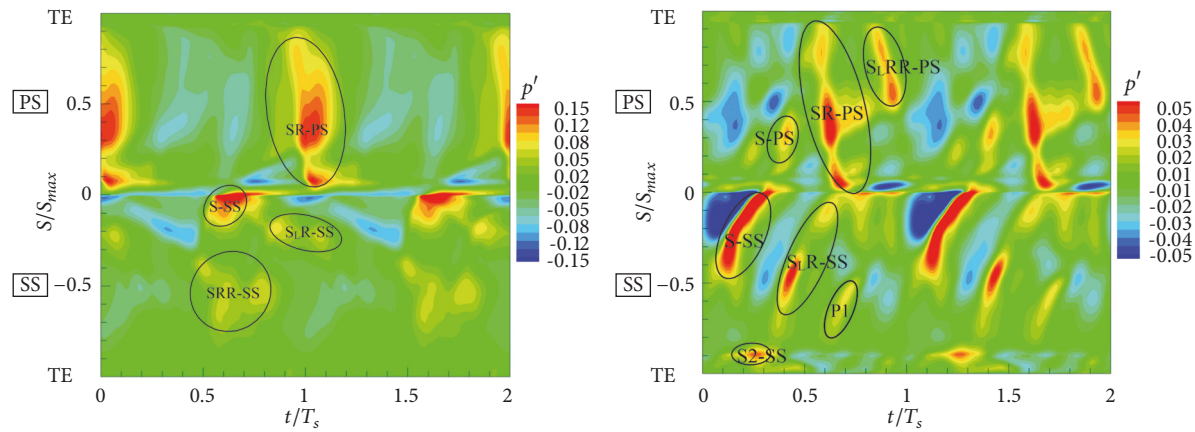

(a) Midspan of -5° vane case

(b) Midspan of +5° vane case

Figure 9: Space-time plots of the unsteady pressure for the VGT at midspan.

space-time plot of the unsteady pressure at low expansion ratio condition in Figure 6(a), it is visualized that the pressure fluctuation peaks appear only once per vane passing period and are associated with the periodically experience of the upstream potential field of the vane. The amplitude of the overall pressure fluctuation and the amplitude of the first vane passing frequency (1BPF) are nearly identical along the blade surface, indicating that the unsteady pressure on the rotor blade at low expansion ratio condition is caused by the flow distortions related to the 1BPF, and the pressure fluctuation energy at higher harmonics is negligible. At nominal expansion ratio condition, the impact of the vane TE shock excitation introduces strong pressure fluctuation peaks about three times of the potential excitation at low expansion ratio condition at the rotor front suction side.

It is suggested that the pressure fluctuation amplitude at second and third BPF are more prominent at the rotor front suction side at transonic condition; the fluctuation amplitude peaks at second and third harmonics are of the same order of magnitude with the overall pressure fluctuation level at the pressure side and aft suction side. In connection with the space-time figure at the nominal expansion ratio condition in Figure 6(b), the increasing appearance of the reflection events is responsible for this phenomenon. The wave reflections across the blade passage lead to the appearance of multiple pressure fluctuation events per vane passing period, leading to higher fluctuation level at higher harmonics.

On the other hand, the reflections distribute the fluctuation energy spatially along the blade surface; the pressure fluctuation levels on the aft suction side and pressure side are increased. On the pressure side and aft suction side, the pressure fluctuation levels are mainly concentrated on 1BPF. With higher vane exit Mach number at high expansion ratio condition, the proportion of the fluctuation at 1BPF reduces compared with the low expansion ratio condition and the fluctuation energy at higher harmonics are more prominent. Moreover the strong spatial pressure gradient introduced by the shock formation is effectuated as a temporal pressure gradient on the blade surface. Both contribute to significant increasing fluctuation energy in multiples of the vane passing frequency.

4. Aerodynamic Excitations for VGT

The pressure fluctuation amplitude variations with respect to the expansion ratios for the design vane stagger angle position (0°) have been analyzed qualitatively and quantitatively to understand the pressure excitation mechanisms on the rotor blade at different operating conditions. For the VGT in this study, variation of the vane stagger angle positions will result in significantly different pressure excitation behaviors on the rotor blade surface. On one hand, mismatch of the velocity triangle of the elementary stage due to the vane stagger angle variation will lead to the deterioration of the turbine performance, and extra pressure fluctuation events may be introduced by the incidence variation. Meanwhile the degree of reaction of the VGT will significantly change, shown in Table 2. The Mach numbers at the stator and rotor exits are different at different vane stagger angle conditions due to different expansion rate of the flow in the stator and rotor blade row, which will significantly affect the aerodynamic excitation mechanisms on the rotor blade surface. To evaluate the effect of variations of the vane stagger angle positions on the rotor blade excitation levels, the qualitative and quantitative analysis of the unsteady pressure on the rotor blade of VGT will be given in this section.

4.1. Unsteady Pressure Distribution at Midspan for VGT. The phenomenological identification and classification of the rotor blade excitations are established with the aid of the space-time plot of the pressure fluctuation on the rotor blade at the design vane condition. To analyze the effect of vane stagger angle variations on the pressure fluctuation events and amplitudes of the rotor blade surface, the space-time plots of the normalized pressure fluctuation at -5° and +5° vane positions at nominal total-to-static pressure ratio condition (P_{t0}/P_{s2}=3.41) are present in Figure 9.

It is observed in Figure 9(a) that the pressure fluctuation distribution at midspan of the closed vane case is similar to the 0° vane position in Figure 6(b). It is suggested in Table 2 that the degree of reaction at -5° vane condition is lower, indicating higher expansion in the stator passage

and lower expansion in the rotor passage. The vane exit Mach number increases at the -5° vane condition, resulting in a stronger vane TE shock strength. The amplitude of the pressure fluctuation peak S-SS at the front suction surface is comparable to the 0° vane condition, but length of the region with high fluctuation level on the rotor LE is greatly reduced. However, the amplitude and range of the pressure fluctuation peak related to the shock wave reflection SR-PS, emanating from the suction side to the neighboring pressure side, are amplified significantly, and the magnitude of the pressure fluctuation peak SR-PS is comparable with the direct impact of the right running vane TE shock S-SS. This is due to the variation of the inflow incidence and the shock strength. The reflected shock impinges on the pressure side and reflects toward the aft suction side of the neighboring rotor blade; the associated pressure fluctuations peak is marked SRR-SS in the time-space plot. Due to lower degree of reaction at -5° vane condition, the rotor exit Mach number is only 0.62. This explains the reason that no pressure fluctuation peak related to the rotor TE shock is observed at the rear of the rotor blade.

Figure 9(b) suggests that the amplitude of the pressure fluctuation on the suction side at +5° vane condition decreases significantly compared to the 0° and -5° vane conditions at nominal expansion ratio. Due to lower expansion rate in the vane passage at +5° vane condition with larger degree of reaction, the vane exit Mach number is lower, indicating that the unsteady excitation related to the impact of the vane TE shock is relatively low. The pressure fluctuation amplitude related to the impact of the incident and reflected shocks at +5° vane condition is comparable to the subsonic case at 0° vane position in Figure 6(a).

Meanwhile the effect of the left running shock wave is more prominent at +5° vane condition due to changed wave reflection angle. The reflected left running shock wave impinges on the rotor suction side, and the pressure peak designated S_LR-SS follows its path. It reflects toward the pressure surface of the neighboring blade, which corresponds to the pressure fluctuation peak S_LRR-PS at aft pressure side. The degree of reaction at +5° vane condition is around 0.42, which means the expansion in the rotor passage is large. It can be seen in Table 2 that the rotor exit Mach number is transonic, and this leads to the high pressure fluctuation level region named S2-SS at rear suction side.

Propagation and reflection of left and right running legs of the vane TE shock result in the complex distributions of the unsteady pressure on the rotor blade surface at +5° vane condition. More comparable pressure distortion events exist per vane passing period with lower amplitude. There is a significant difference with the subsonic case at 0° vane condition, though the amplitude is comparable.

It can be concluded from Figure 9 that the variation of the pressure fluctuation patterns at different vane stagger angles is mainly affected by the vane exit Mach numbers. For the closed vane conditions, the vane exit Mach number increases with larger expansion rate in the vane passage, and the vice versa for the open vane condition. The variation of the flow expansion in the rotor passage will also add to the overall difference. The effect of the incidence variation is very minor.

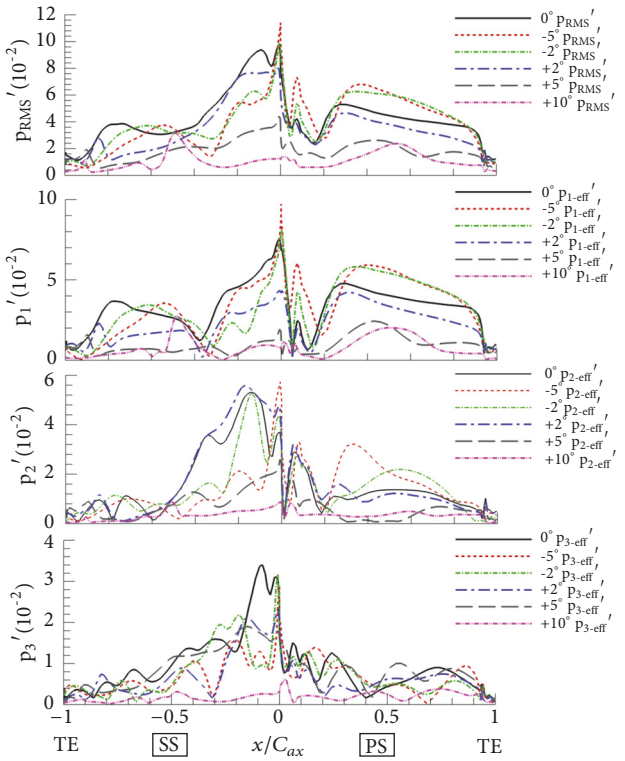

Figure 10: Pressure amplitude distribution along the rotor blade midspan at nominal pressure ratio of VGT.

Predicted pressure fluctuation amplitude levels at the midspan of the rotor blade at six vane positions are shown in Figure 10, for the normalized overall pressure fluctuation RMS and first three harmonics of the vane passing frequency, respectively. Discussion of Figure 10 will start with the analysis of the RMS of the pressure fluctuation (p') in time domain. Pressure peaks at the LE of the rotor blade are mainly related to the direct impact of the vane TE shock. For the closed vane condition, the increased vane exit Mach number causes stronger vane TE shock, and the amplitude of the pressure fluctuation at the rotor LE is slightly increased. While the range of the vane TE shock sweeps from the rotor suction side crown to the LE are reduced at closed vane conditions. This indicates the reason that the pressure fluctuation level at the front suction side corresponding to S-SS is reduced at closed vane conditions. However, due to increased strength of the reflected shock wave on the rotor pressure side, the pressure fluctuation levels on most part of the pressure side are amplified. Vane exit Mach number increases with increasing vane turning angle at closed vane conditions, shown in Table 2.

For the +2° and +5° vane conditions, the flow at the vane exit is transonic. Amplitude of the pressure peaks are reduced due to weakened strength of the vane TE shock.

At +10° vane condition, the flow regime at the vane exit is subsonic, and the pressure fluctuation level on the rotor blade is obviously lower than other conditions. However, high pressure fluctuation peaks are observed at rear suction side and pressure side due to the transonic flow at the rotor TE.

It is suggested that the aerodynamic excitations of VGT are mainly related to the impact of the propagation and reflection of the vane TE shock in the blade passage. Variation of the vane TE shock strength at different vane stagger angles results in the different patterns and amplitudes of the unsteady pressure on the rotor blade surface. In addition, the pressure fluctuation due to the rotor TE shock adds to the overall aerodynamic excitations on the rotor blade.

The distribution of the effective value of the amplitude of the pressure fluctuation in 1BPF (p_1') is in good agreement with the overall pressure fluctuation at the pressure side and rear suction side of the rotor blade for all vane conditions. It can also be validated in the space-time plot, as only one pressure distortion event is observed at these locations. Noticeable difference is observed at the front rotor suction side, where the amplitudes of the pressure fluctuation level in higher harmonics are more prominent. Higher harmonic amplitude peaks on the rotor blade are caused by multiple pressure distortion events occurring successively per vane passing period. It is visualized that pressure fluctuation peak at around $0.2\,C_{ax,R}$ of the suction side is very high at 0° and ±2° vane conditions, of which the amplitude is approximately 6% of the stage inlet total pressure. This peak corresponds to the successive experiencing of reflected left running shock and the right running shock impingement on suction surface per vane passing period. At closed vane conditions, for both -2° and -5°, the pressure fluctuation peaks in second harmonic exist on pressure side; this peak is associated with the stronger shock reflection. Amplitude of the pressure peaks increases with increasing closed angle of the vane.

The third harmonic amplitude peak at 0° vane condition at rotor front suction side is obvious. However, the peak values are minor at other vane conditions.

To evaluate the relative strength of pressure fluctuation events in frequency domain, which is connected to 1BPF and higher harmonics, Fourier transformation of the unsteady pressure field is obtained in time at midspan of the blade surface. A global measurement for the pressure fluctuation in a specific BPF at a defined span position is defined as follows:

$$RMS_{\mathrm{n}} = \sqrt{\frac{\int_{\mathrm{arc}} {p'_{\mathrm{n-amp}}}^{2}\,\mathrm{d}s}{2\int_{\mathrm{arc}} \mathrm{d}s}} \tag{2}$$

The pressure fluctuation in a specific BPF RMS_{n} is normalized with the total pressure at the stage inlet.

Normalized pressure fluctuation strength of the overall and first three BPF for six vane stagger angles at four total-to-static pressure ratios is plotted in Figure 11.

For all vane conditions, the pressure excitation levels at low expansion ratio are in the same order of magnitude due to subsonic regime at vane exit, and fluctuation strength in higher harmonics is negligible, which reveals that the pressure fluctuation induced by the vane potential field and wake are mainly concentrated on the first vane passing frequency.

For the design and closed vane conditions, the overall pressure fluctuation RMS level in time domain increases with increasing pressure ratio, the pressure fluctuation levels at nominal and high expansion ratios are almost three times of low expansion ratio conditions. The normalized pressure fluctuation RMS for the nominal and high pressure ratios are nearly the same. Variation of the overall pressure fluctuation RMS levels at closed and design vane conditions is not evident.

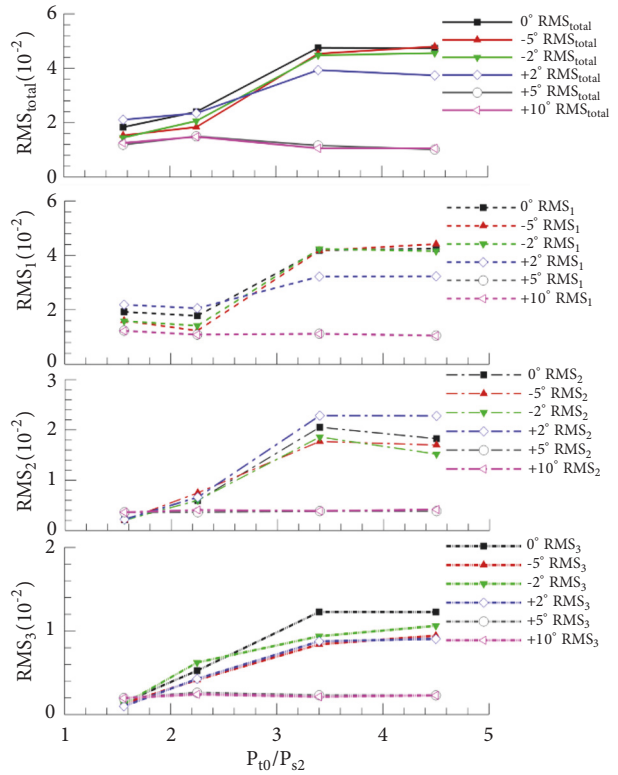

Figure 11: RMS pressure fluctuation at the midspan of VGT at various pressure ratio.

Trend of the pressure fluctuation RMS in the first BPF is similar to the overall RMS, though the amplitude is slightly lower. The pressure fluctuation in multiples of the BPF becomes more prominent; it is observed in Figure 11 that the pressure fluctuation in second harmonic at nominal and high expansion ratio conditions are of the same order of magnitude with the overall RMS of the pressure fluctuation at the low and medium expansion ratio conditions. The strength of the second and third harmonic of BPF increases with the increasing pressure ratio for the design and closed vane conditions.

For the open +5° and +10° vane conditions, the pressure fluctuation level keeps almost constant at relatively low level for all simulated pressure ratio conditions. The pressure fluctuation mainly attributes to the fluctuation related to the first BPF, and the excitation levels of higher harmonics are negligible.

For the open +2° vane condition, the trend of the pressure fluctuation RMS with respect to the pressure ratio is similar to the closed and design vane conditions. The pressure fluctuation level in second harmonic is higher than the design and closed vane conditions at nominal and high expansion ratio, which is indicated in Figure 10.

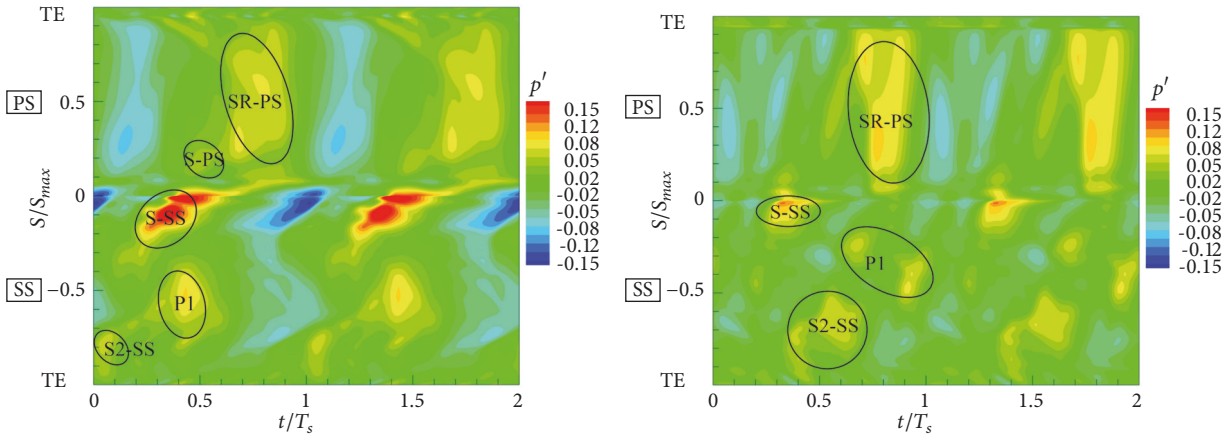

(a) Pressure fluctuation at 5% span

(b) Pressure fluctuation at 95% span

Figure 12: Space-time plots of the unsteady pressure at endwall regions at design vane condition with nominal expansion ratio.

4.2. Spanwise Variations of the Pressure Fluctuation of VGT. Based on the link of pressure fluctuation on the rotor blade surface and the flow distortions in the rotor passage at midspan, the spanwise variations of the pressure fluctuation in VGT are investigated. The pressure fluctuation distributions at 5% and 95% span locations are selected. On one hand, vane exit Mach number decreases from hub to tip; on the other hand, the complex secondary flow and vortical structures near the endwall regions may add to the aerodynamic excitations. Discussion of the spanwise variation of the pressure fluctuation on the rotor blade surface is based on the analysis of the design vane condition at nominal pressure ratio in Figure 12.

For the design vane condition at nominal expansion ratio, the pressure fluctuation events at the hub are all observed at midspan, though the fluctuation amplitude and range are slightly changed. At the hub region, strength of the vane TE shock is slightly stronger than the midspan due to higher vane exit Mach number; however the range of the vane TE shock wave moving on the rotor SS is reduced. Due to the increased shock strength and the geometry of the rotor hub, the range of the pressure fluctuation peak SR-PS, corresponding to the shock reflection emanating from the rotor SS to the neighboring rotor PS, is enlarged, but the strength is reduced. In connection with the distribution of the overall pressure fluctuation and the pressure fluctuation related to multiples of BPF in Figure 13(a), the distribution of the pressure fluctuation in 1BPF is nearly the same with the overall pressure fluctuation. Apart from the LE of the rotor suction side, the pressure fluctuation amplitudes at second and third harmonic are very low. It suggests that the main pressure fluctuation derives from the flow distortion associated with 1BPF at the hub region.

The situations of the pressure fluctuation distributions at hub region at closed and open +2° vane conditions are in accordance with the design vane condition. For the open +5° and +10° vane conditions, the pressure fluctuation attributes to amplitude at the first BPF mostly; the pressure fluctuation amplitude at higher harmonics is negligible, which is the same with the conclusion at midspan.

At the tip region for the design vane condition, it is observed that the distribution of the unsteady pressure is different from the lower span positions. Due to reduced shock strength and larger axial gap at the vane tip region, the shock induced pressure fluctuation is rather weak at the front SS of the rotor blade compared to the lower spans. Range and amplitude of pressure fluctuation peak S-SS are lower in the tip region. Combining the distribution of the pressure fluctuation amplitude in the tip region in Figure 13(b), we can see that the pressure amplitude related to the direct impact of the vane TE shock at the front SS is of the same order of the magnitude with the pressure fluctuation events at the aft SS and PS. It is also observed that the pressure fluctuation peak in second harmonic is of the same order with the fluctuation in 1BPF at the LE of the suction side, but the range of the high pressure fluctuation level at second harmonic is larger compared to the first BPF. At the front rotor suction side at 95% span, more pressure fluctuation events appear per vane passing period, resulting in a high peak of the pressure fluctuation at second harmonic. Only one pressure fluctuation event is seen on the pressure side and aft suction side of the rotor blade surface per vane passing period, which is shown in Figure 13(b) that the pressure fluctuation peak at second harmonic is low.

Therefore, it is concluded that, at the front SS of the rotor tip region, the pressure fluctuation attributes to the blend of the fluctuation of first and second harmonics. The unsteady pressure characteristics for the closed vane condition at the tip region are similar to the design condition, though the amplitude of the pressure fluctuation is higher due to higher exit Mach number at the tip region of the vane exit.

Normalized pressure fluctuation RMS of the overall and first three h at endwall regions for six vane stagger angles at four total-to-static pressure ratios is plotted in Figure 14.

Trends of the normalized pressure fluctuation RMS versus the expansion ratio at different vane stagger angle conditions at the hub and tip regions are basically the same with the midspan. It is visualized that the overall pressure fluctuation RMS at the tip region is lower compared to the

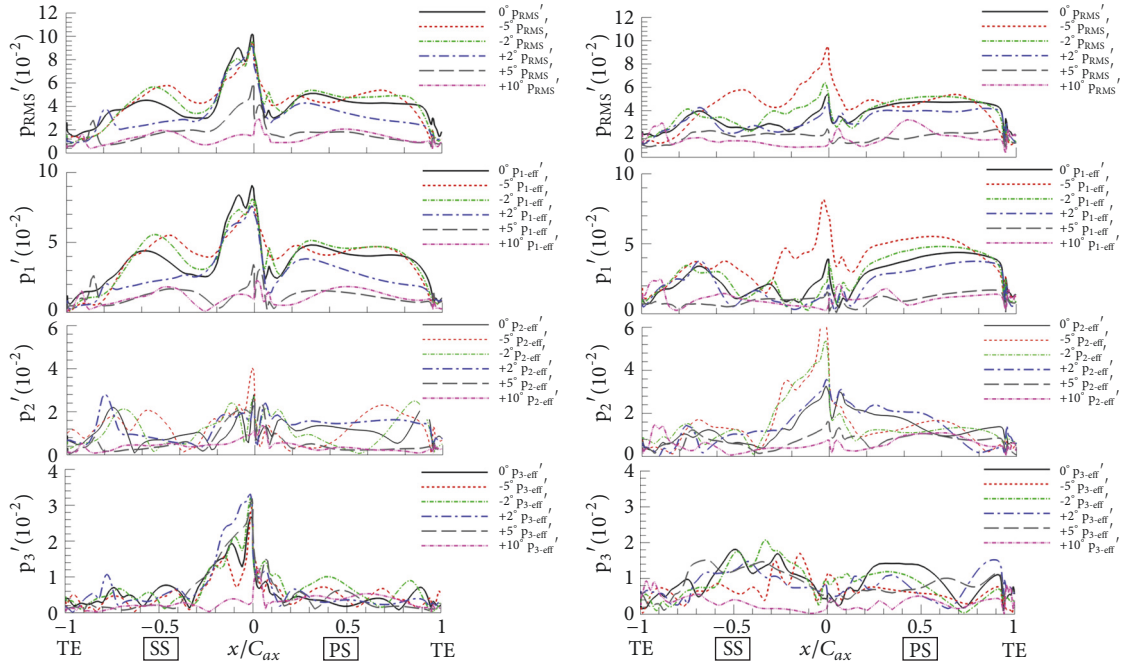

(a) Pressure fluctuation at 5% span

(b) Pressure fluctuation at 95% span

Figure 13: Pressure fluctuation distribution along the rotor blade surface at endwall regions.

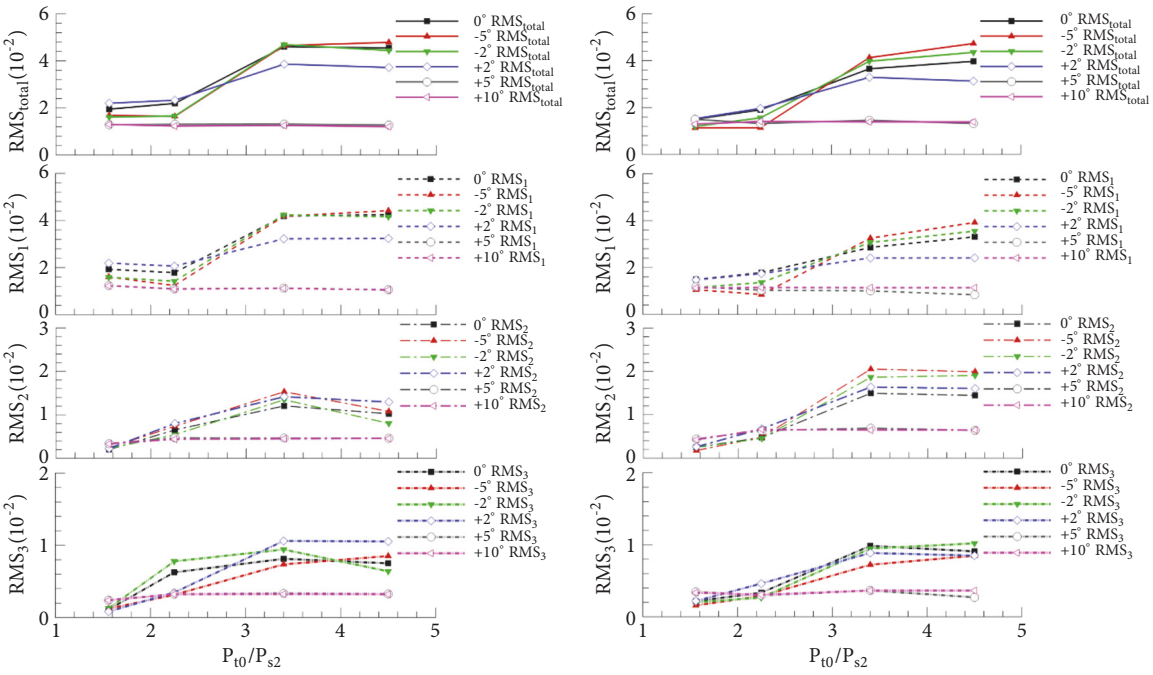

(a) RMS at 5% span

(b) RMS at 95% span

Figure 14: RMS of the pressure fluctuation at endwall regions.

lower span positions and the RMS level are basically the same at the midspan and hub region. However, for the RMS of the pressure fluctuation at 1BPF slightly decreases from hub to tip along the rotor blade, which is related to the shock strength variations along the spanwise.

Based on Plancherel Theorems, the global pressure fluctuation energy in 1BPF accounts for 82.6% of the overall pressure fluctuation energy for the design vane stagger at nominal expansion ratio. However, the corresponding proportions at 50% and 95% span for design vane condition

are 61.1% and 59.8%, respectively. This indicates that the pressure fluctuation energy is more concentrated on the first vane passing frequency at the hub region compared to the midspan. Moreover, the fluctuation energy is more distributed to higher harmonic at higher spans.

5. Conclusions

Unsteady simulations adopting SAS SST model have been performed in variable geometry turbine with six vane stagger angles at four expansion ratios. As the results suggest:

(1)The blade excitation mechanisms are directly dependent on the operating conditions of the stage in terms of vane exit Mach numbers for all test cases. At subsonic condition, the blade pressure fluctuations are related to the potential filed and wake propagation, and the excitation level is very low. At transonic condition, the vane trailing edge shock causes additional disturbance and is the dominating excitation source; the global pressure fluctuation amplitude is three times of the subsonic condition.

(2) The pressure fluctuation energy at higher vane exit Mach number conditions is more prominent. With increasing Mach numbers, the propagation and reflections of the vane trailing edge shock lead to more pressure distortion events per vane passing period, and the energy of the pressure fluctuation is distributed to higher harmonics.

(3)The variation of the aerodynamic excitations on the rotor blade at different vane stagger angles is caused by the variation of the expansion in the stator and rotor passage. Due to varied reaction of degree at different vane stagger angles, the changing Mach numbers at exit of vane and rotor cause different patterns of unsteady pressure on the rotor blade. The aerodynamic excitations at open vane conditions are reduced due to lower vane exit Mach numbers, but the global aerodynamic excitations are not increased at closed vane conditions.

(4)Spanwise variation of the pressure fluctuation patterns on is observed. Pressure fluctuation energy is more concentrated on the first vane passing frequency at the hub region. Fluctuation energy is more distributed to higher harmonic at higher spans.

Nomenclature

BPF: Blade passing frequency
C_a: Axial component of absolute velocity [m/s]
$C_{ax,S}$: Axial chord of stator vane [m]
$C_{ax,R}$: Axial chord of rotor blade [m]
ΔH : Enthalpy drop [J/kg]
Δr: Tip clearance of rotor blade
γ: Stagger angle[°]
LE: Leading edge
Ma_1: Vane exit Mach number
$Ma_{2,r}$: Rotor exit relative Mach number
n: Rotor speed [r·min^{-1}]
P-PS: Potential impact on rotor pressure side
P-SS: Potential impact on rotor suction side
PR-SS: Potential reflection on rotor suction side
p' : Fluctuation pressure [Pa]
$p'_{n-\mathrm{amp}}$: Pressure amplitude of nth BPF [Pa]
p'_{n-eff}: Effective value of the pressure fluctuation related to nth BPF [Pa]
P_{s2}: Total pressure at stage outlet [Pa]
P_{t0}: Total pressure at stage inlet [Pa]
Re_c: Reynolds number
RMS: Root mean square
RMS_{total}: Global fluctuation strength
RMS_n: Fluctuation strength related to nth BPF
Ω: Reaction degree
S-PS: Vane TE shock impact on rotor pressure side
S-SS: Vane TE shock impact on rotor suction side
S_2-SS: Rotor TE shock impact on rotor suction side
SR-PS: Shock reflection on rotor pressure side
S_LR-SS: Vane TE left running shock reflection on rotor pressure side
Ts: Vane passing period [s]
TE: Trailing edge
U: Circumferential velocity [m/s]
VGT: Variable geometry turbine
Z: Blade count
η_T: Total-to-total turbine efficiency.

Data Availability

The data used to support the findings of this study are available from the corresponding author upon request.

Conflicts of Interest

The authors declare that they do not have any commercial or associative interest that represents conflicts of interest in connection with the manuscript submitted.

Acknowledgments

The research of this article was supported by "the Fundamental Research Funds for the Central Universities" (no. 3102019ZX027).

References

[1] R. Dénos, T. Arts, G. Paniagua, V. Michelassi, and F. Martelli, "Investigation of the unsteady rotor aerodynamics in a transonic turbine stage," *Journal of Turbomachinery*, vol. 123, no. 1, pp. 81–89, 2001.

[2] R. J. Miller, R. W. Moss, R. W. Ainsworth, and C. K. Horwood, "Time-resolved vane-rotor interaction in a high-pressure turbine stage," *Journal of Turbomachinery*, vol. 125, no. 1, pp. 1–13, 2003.

[3] O. P. Sharma, G. F. Pickett, and R. H. Ni, "Assessment of unsteady flows in turbines," *Journal of Turbomachinery*, vol. 114, no. 1, pp. 79–90, 1992.

[4] O.P. Sharma, R. H. Ni, and S. Tanrikut, "Unsteady flows in turbines: Impact on design procedure," Agard, Turbomachinery Design Using Cfd 27 P1994.

[5] E. Willis and A. Welliver, "Variable-cycle-engines for supersonic cruising aircraft," in *Proceedings of the AIAA/SAE 12th Propulsion Conference*, AIAA/SAE, 1976.

[6] D. H. Silvern and W. R. Slivka, "Analytical investigation of turbines with adjustable stator blades and effect of these turbines on jet-engine performance," Tech. Rep., Technical Report Archive & Image Library, 1950.

[7] T. Moffitt, H. Schum, and W. J. Whitney, "Performance of a single-stage turbine as affected by variable statorarea," in *AIAA*, pp. 69–525, 1969.

[8] E. H. Razinsky and W. R. Kuziak, "Aerothermodynamic performance of a variable nozzle power turbine stage for an automotive gas turbine," *Journal of Engineering for Gas Turbines and Power*, vol. 99, no. 4, pp. 587–592, 1977.

[9] C. Bringhenti and J. R. Barbosa, "Methodology for gas turbine performance improvement using variable-geometry compressors and turbines," *Proceedings of the Institution of Mechanical Engineers, Part A: Journal of Power and Energy*, vol. 218, no. 7, pp. 541–549, 2004.

[10] C. Qiu, H. F. Song, and S. L. Weng, "Linear perturbation method for performance analysis of variable geometry gas turbines," *Journal of the Energy Institute*, vol. 82, no. 3, pp. 168–175, 2009.

[11] C. Qiu, F Song, H Wang et al., "Performance estimation of variable geometry turbines," *Proceedings of the Institution of Mechanical Engineers Part A Journal of Power & Energy*, vol. 223, pp. 441–449, 2009.

[12] J. Gao, Q. Zheng, G. Yue, and F. Wang, "Variable geometry design of a high endwall angle power turbine for marine gas turbines," in *Proceedings of the ASME Turbo Expo: Turbine Technical Conference &; Exposition*, 2015.

[13] J. Gao, W. Fu, F. Wang et al., "Experimental and numerical investigations of tip clearance flow and loss in a variable geometry turbine cascade," *Proceedings of the Institution of Mechanical Engineers Part A Journal of Power & Energy*, vol. 232, no. 2, 2017.

[14] J. Gao, Q. Zheng, Z. Zhang, and Y. Jiang, "Aero-thermal performance improvements of unshrouded turbines through management of tip leakage and injection flows," *Energy*, vol. 69, pp. 648–660, 2014.

[15] J. Gao, M. Wei, P. Liu, G. Yue, and Q. Zheng, "Improved clearance designs to minimize aerodynamic losses in a variable geometry turbine vane cascade," *ARCHIVE Proceedings of the Institution of Mechanical Engineers Part C Journal of Mechanical Engineering Science 1989-1996*, vol. 203-210, 2017.

[16] R. Balasubramanian, S. Barrows, and J. P. Chen, "Investigation of shear-stress transport turbulence model for turbomachinery applications," in *Proceedings of the AIAA Aerospace Sciences Meeting and Exhibit*, 2013.

[17] F. R. Menter and Y. Egorov, "A scale adaptive simulation model using two-equation models," in *Proceedings of the Aiaa Aerospace Sciences Meeting and Exhibit*, 2005.

[18] F. R. Menter and Y. Egorov, "The scale-adaptive simulation method for unsteady turbulent flow predictions. part 1: theory and model description," *Flow, Turbulence and Combustion*, vol. 85, no. 1, pp. 113–138, 2010.

[19] J. Liu, W. Qiao, and W. Duan, "Effect of bowed/leaned vane on the unsteady aerodynamic excitation in transonic turbine," *Journal of Thermal Science*, vol. 28, no. 2, pp. 133–144, 2019.

[20] W. T. Hou, W. Y. Qiao, and H. L. Luo, "Shock-wave/boundary-layer interaction in a transonic turbine cascade," *Proceedings of the Institution of Mechanical Engineers, Part G: Journal of Aerospace Engineering*, vol. 225, no. 1, pp. 77–85, 2011.